Solid State Ionics 277 (2015) 77–82

Contents lists available at ScienceDirect

Solid State Ionics

journal homepage: www.elsevier.com/locate/ssi

Water interaction with perfect and fluorine-doped Co_3O_4 (100) surface ☆

G.A. Kaptagay [a,*], T.M. Inerbaev [a], Yu.A. Mastrikov [b], E.A. Kotomin [b], A.T. Akilbekov [a]

[a] L.N. Gumilyov Eurasian National University, Mirzoyan str. 2, Astana, Kazakhstan
[b] Institute of Solid State Physics, University of Latvia, Kengaraga str. 8, Riga, Latvia

ARTICLE INFO

Article history:
Received 22 June 2014
Received in revised form 10 March 2015
Accepted 11 March 2015
Available online 3 April 2015

Keywords:
Co_3O_4
Spinel oxide
Water sorption
Free-energy diagram
Surface

ABSTRACT

We report the results of theoretical investigations of water adsorption on undoped and fluorine-doped Co_3O_4 (100) surface by means of the plane-wave periodic density functional theory (DFT) calculations combined with the Hubbard-*U* approach and statistical thermodynamics. We discuss the effect of fluorine-doping of the Co_3O_4 (100) surface and calculated oxygen evolution reaction overpotential based on the Gibbs free-energy diagram of undoped and F-doped surfaces.

© 2015 Elsevier B.V. All rights reserved.

1. Introduction

The increasing consumption of energy in the world has stimulated an intensive research of different sources of renewable energy. This includes research on the electrochemical splitting of water, in order to increase the efficiency of the oxygen evolution reaction (OER) by means of reducing overpotential. The interaction of water with transition metal oxide surfaces plays an important role in catalysis, surface chemistry, gas sensors [1], and photo- and electrochemistry [2,3]. One of the promising materials for water splitting is spinel-type tricobalt tetra oxide, Co_3O_4. Recently, Norskov et al. combined DFT + *U* calculations and atomistic thermodynamics in theoretical study of the OER activity on pure Co_3O_4 and β-CoOOH (0112) surfaces as a function of applied potential and pH [4]. Catalyst performance could be, in principle, improved using different promoters [5–7]. In particular, Xu et al. [8] presented a comparative experimental study of water adsorption on pure and cation, Al-doped Co_3O_4. It is also well known that the presence of different promoters in p-type semiconducting photocatalysts, such as Co_3O_4, could lead to a significant decrease of the OER overpotential [9]. Indeed, in an experimental study by Gasparotto et al. [10] anion, F-doping of nanostructured films of Co_3O_4 resulted in a significant improvement of catalytic properties. It is expected that this is related to an increase of concentration of Co^{2+} active centers. Motivated by the latter experiments, in the present study we analyzed the catalytic activity of different Co-sites on the pure and F-doped Co_3O_4 (100) surface in H_2O adsorption.

Since the atomistic mechanism of the OER is complicated and not fully studied, insights into the thermodynamics of the reaction could be important, e.g. using the well-established approach developed by Norskov and co-workers [11–13]. Their OER process consists of four elementary reaction steps, each involving the coupled transfer of an electron to the electrode and a proton to water (the * indicates molecules at the surface) [9]

$$H_2O + * \rightarrow OH^* + H_2O + e^- + H^+ \quad (1)$$

$$OH^* + H_2O \rightarrow O^* + H_2O + e^- + H^+ \quad (2)$$

$$O^* + H_2O \rightarrow OOH^* + e^- + H^+ \quad (3)$$

$$OOH^* \rightarrow O_2 + e^- + H^+. \quad (4)$$

In order to calculate the energetics of this process, the Gibbs free energies of H_2O adsorption and of the intermediate products (O, OH, OOH) should be calculated.

2. Method and surface model

2.1. Computational methodology

The calculations have been performed using the ab initio plane wave computer code VASP [14,15] using the projector-augmented plane-wave (PAW) formalism [16] in conjunction with PBE (Perdew–Burke–Ernzerhof) GGA exchange-correlation functional [17]. The standard Monkhorst–Pack grid with the 4 × 4 × 4 sampling mesh for the bulk calculations and the 2 × 2 × 1 for the slab calculations was used [18]

☆ The paper was presented at EMRS2014.

* Corresponding author.
E-mail address: kaptagai.gulbanu@mail.ru (G.A. Kaptagay).

http://dx.doi.org/10.1016/j.ssi.2015.03.012
0167-2738/© 2015 Elsevier B.V. All rights reserved.

Table 1
The calculated lattice constant (Å), bond distances (Å), heat of formation (kJ/mol), band gap (eV), and exchange coupling J (10^{-4} eV). The results of other calculations are presented for comparison.

Method	Lattice constant (Å)	Distance Co^{2+}–O^{2-} (Å)	Distance Co^{3+}–O^{2-} (Å)	Heat of formation (kJ/mol)	Bandgap (eV)	Exchange coupling J (10^{-4} eV)
PBE + U (this work)[a]	8.15	1.96	1.93	−894	1.60	−12
PBE [22]	8.19	1.95	1.93	−683	1.39	−25
PBE + U [22][b]	8.27	1.93	1.95	−884	1.96	+1
PBE0 [22]	–	–	–	–	3.42	−50
Exp. [23]	8.08	1.93	1.92	−891	1.65	−6.26

[a] Exchange coupling constant J was calculated with the cutoff energy of 800 eV and with the sampling mesh 4 × 4 × 4.
[b] Two different U-parameters (4.4 eV and 6.7 eV) used for Co^{2+} and Co^{3+} ions, respectively.

along with the cutoff energy of 600 eV and the Methfessel–Paxton [19] smearing with $\sigma = 0.1$ eV. In performed calculations for the periodic slab model (infinite in two dimensions) the positions of all ions were fully relaxed, to render the net forces acting upon the ions smaller than 1×10^{-2}eV · Å^{-1}. In order to avoid the interaction between periodically translated images along the direction normal to the surface, we used vacuum gap of 12 Å.

Co_3O_4 has a spinel structure ($Fd\bar{3}m$) which contains half-filled octahedral sites with Co^{3+} (d^6) cations and tetrahedral sites with Co^{2+} (d^7) cations, which are four-fold-(Co_{4f}) and three-fold-(Co_{3f}) coordinated at the (100) surface, respectively, whereas all surface oxygen ions are equivalent. One unit cell in the bulk contains 2 formula units, i.e. 14 ions. In this study, we focus on the water interaction with the Co_3O_4 (100) surface. The layer was defined by the subset of the ions lying in the same plane perpendicular to the given Miller index in the idealized spinel structure.

We simulated symmetric slabs with an odd number of layers, for which the total dipole moment is zero. As the number of slab layers exceeds seven, the atomic relaxation and the surface energy finally converge. This slab is stoichiometric and symmetric along the surface normal plane. Totally, the 7-plane slabs contain 70 ions.

2.2. Thermodynamic description

In thermodynamic modeling the free enthalpy of a surface (A) as a function of the thermodynamic parameters (T, p) and the number of adsorbed molecules n_i^{ads} could be found using a general expression:

$$G^a_{hkl}(T,p,\theta) = \frac{1}{A}\left[G^{slab}\left(T,p,\left\{n_i^{ads}\right\}\right) - \sum_i n_i^{ads}\mu(T,p)\right] \quad (5)$$

where $\mu(T, p)$ is the chemical potential of water.

The minimum of a given function $\Delta_a G_{hkl}(p, T, nH_2O)$ is not searched directly. Adsorption process can be as expressed:

$$Co_3O_4(hkl) + nH_2O \leftrightarrow Co_3O_4(hkl)/\{nH_2O\}\ . \quad (6)$$

The related adsorption Gibbs energy, $\Delta_a G_{hkl}(p, T)$, can be defined as

$$\Delta_a G_{hkl}(p,T,nH_2O) = G^s(Co_3O_4(hkl)/\{H_2O\}) - \left[G^s(Co_3O_4(hkl)) + G^g(H_2O)\right] \quad (7)$$

where $G^g(H_2O) = n\mu(H_2O)$. Assuming that the vibrational terms of the surface do not vary significantly upon water adsorption ($\Delta G^s \cong \Delta E^{el}$), one can factorize the free energy of adsorption in two parts: the electronic contribution, $\Delta_a E^{el}$, calculated as difference of the corresponding static DFT energies at 0 K, and the change in the chemical potential of water molecules upon adsorption:

$$\Delta_a G_{hkl}(p,T,nH_2O) = \Delta_a E^{el} - n\Delta\mu(H_2O) \quad (8)$$

where $\Delta_a E^{el} = E^{el}(Co_3O_4(hkl)/\{H_2O\}) - E^{el}(Co_3O_4(hkl)) - nE^{el}(H_2O)$.

In turn, changes in the chemical potential of a gas phase and adsorbed water are described in a standard way:

$$\Delta\mu(p,T) = \Delta\mu^0(T) + RT\ln\left(p/p^0\right) \quad (9)$$

and can be computed using standard statistical thermodynamics:

$$\Delta\mu^0(T) = \Delta\left[E_{ZPE} + E^{osc}(0\rightarrow T) + E^{rot} + E^{trans}\right] + RT - T\left(S^{osc} + S^{rot} + S^{trans}\right). \quad (10)$$

Those thermal contributions cover changes in the translational, rotational, and vibrational degrees of freedom upon adsorption of n molecules. In the adsorbed state the parent gas-phase translations and rotations are converted into low-frequency soft oscillations (so-called frustrated rotations and translations), whereas the hard stretching OH modes were only slightly modified (by 20 cm^{-1} toward lower values) when water adsorbs associatively and by about ~200 cm^{-1} for dissociative mode of adsorption. The frustrated modes due to strong binding of H_2O to the surface exhibit rather elevated, as for those type of molecular motion, frequencies of 200–300 cm^{-1}. However, the contribution to entropy and energy changes from the frustrated modes are quite small, and the major part of the thermal contribution to the chemical potential of the adsorbed water species comes from hard vibrations and is approximated by zero-point energy of the gas-phase H_2O molecule:

$$\Delta\mu^0(T,p) = \mu^0(T) - E^g_{ZPE}(H_2O) + T\ln\left(p/p^0\right). \quad (11)$$

The pressure term in expression (11) was corrected by using virial expansion, up to the first power of the molar volume:

$$pV_m = RT(1 + B/V_m). \quad (12)$$

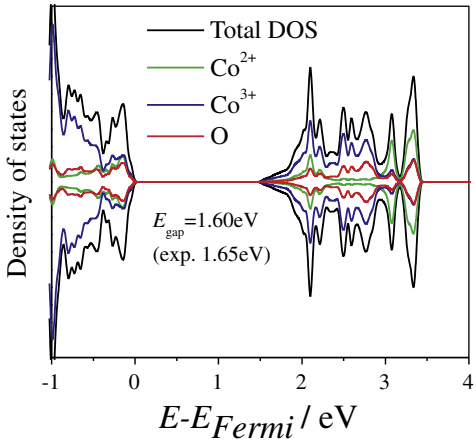

Fig. 1. The electronic DOS of a pure Co_3O_4.

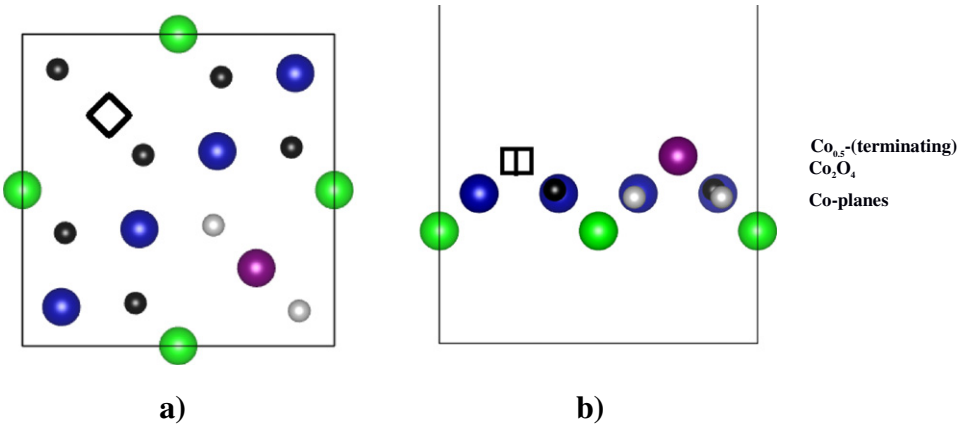

Fig. 2. Co_3O_4 (100) $Co_{0.5}$-terminated surface top view (a) and side view (b). Color coding: Co°_{5c}, blue; Co^{T}_{4c}, green; Co^{T}_{2c}, purple; O_{3c}, black; O_{4c}, gray; The empty cube indicates Co site.

3. Results

3.1. Determination of the Hubbard parameter U

In this work the electron correlation effects were accounted using the rotationally invariant formulation of the on-site model by Dudarev et al. [20]. In previous studies on pure Co_3O_4 [4,9] the Hubbard-U parameter of 3.5 eV was used. We optimized the effective U parameter (corresponding to $U_{eff} = U - J$ in the original GGA + U formulation) for Co ions and found that the parameter $U_{eff} = 3$ eV reproduces very well both the experimental structural parameters as well as the band gap—see Table 1 and Fig. 1.

The self-consistent magnetic moments on Co^{2+} and Co^{3+} ions are 2.63 μ_B and zero, respectively, to be compared with 2.61 μ_B obtained in previous PBE calculations, Ref. [21]. Fig. 1 presented the electronic DOS of a pure Co_3O_4.

The optimized lattice constant of Co_3O_4 spinel structure, $a_0 =$ 8.312 Å and the internal u parameter (position of oxygen anions in the unit cell) of 0.268 are in good agreement with the experimental values of 8.082 Å and 0.263, respectively. Octahedral cobalt–oxygen and tetrahedral cobalt–oxygen bond lengths were equal to $d^{O}_{Co-O} = 1.942$Å and $d^{T}_{Co-O} = 1.963$Å are close to the experimental ones $d^{O}_{Co-O} = 1.920$Å and $d^{T}_{Co-O} = 1.935$Å.

In our calculations we consider the energetically most stable Co_3O_4 (100) surface. As was shown by Zasada et al. [24], the surface energies (under vacuum conditions) for (100), (110) and (111) surfaces are 1.39, 1.65 and 1.48 $J \cdot m^{-2}$ that is, the most stable is the (100) surface.

Thus, the most stable structure of the terminating (100) plane consists of four coordinationally unsaturated 5-fold Co°_{5c}, two recessed, fully coordinated 4-fold Co^{T}_{4c}, and two protruding 2-fold Co^{T}_{2c}. (Fig. 2). The distance between the nearest Co° ions in a slab is 2.91 Å and the Co^{T} ions are separated by 7.63 Å. There are two types of exposed oxygen ions: the 4-fold O_{4c} and 3-fold O_{3c}. Following [4,21], we modeled the (100) surface with 7 layer symmetrical and stoichiometric slabs shown in Fig. 2. In order to get equivalent both upper and lower terminations, one Co^{T} was moved from the upper plane to the bottom plane. This is why we denote this as $Co_{0.5}$ termination. Thus, the Co_3O_4 (100) surface termination has a composition of $\{1Co^{T}_{2c}, 4Co^{o}_{5c}, 2Co^{T}_{4c}, 6O_{3c}, 2O_{4c}\}$.

The surface energy was calculated as:

$$\gamma = (E_{slab} - nE_{bulk})/(2 * m * s) \quad (13)$$

where E_{slab} denotes the slab energy and nE_{bulk} energy of the corresponding number of Co_3O_4 units in the bulk, m is the number of elementary surface units s. Because the surface system is modeled by a slab with two equivalent surfaces, the surface free energy is multiplied by a factor of 0.5. The calculated GGA + U (100) surface energy is equal to 1.23 $J \cdot m^{-2}$ smaller than 1.39 $J \cdot m^{-2}$, obtained in the GGA calculations [24].

3.2. Water adsorption

In the present study, we studied the catalytic activity of Co^{T}_{2c} and Co^{O}_{5c} sites for H_2O adsorption on the pure and F-doped Co_3O_4 (100) surface. To investigate the effect of fluorine doping, one 3-fold O_{3c} (with one missing bond to Co^{T}) surface oxygen atom was substituted by a fluorine ion as shown in Fig. 3 (The relative $Co^{T}_{2c} - F$ distances are 4.12 Å and 2.14 Å for $Co^{O}_{5c} - F$). Therefore, the F dopant concentration was 12.5%. After fluorine doping the slab structure was reoptimized. The calculations predict no essential lattice relaxation around the substitutional F ion: the change of the equilibrium bond length between O and catalytic active cobalt, $Co^{T}_{2c} - O_{3c}$ is larger than $Co^{T}_{2c} - F$ bond by $\Delta l = 0.001$Å only. The effective F ion charge was $-1.01e$, slightly larger than $-0.96e$ for the host O ion.

We have investigated a large number of starting geometries of water ad-molecule for detection of the most stable adsorption configuration. The most stable sites for water adsorption were found on the most unsaturated Co ions. For water adsorption simulations molecule was added on the top of Co^{T}_{2c} and Co^{O}_{5c} ions at perfect and fluorine doped Co_3O_4 (100) surface. Fig. 4 shows H_2O adsorption geometries at the Co^{T}_{2c} site on the Co_3O_4 (100) surface.

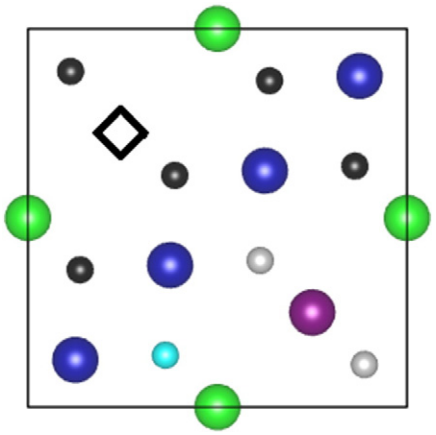

Fig. 3. Top view and side view of fluorine doping on the Co_3O_4 (100) $Co_{0.5}$-terminated surface. Color coding: Co^{O}_{5c}, blue; Co^{T}_{4c}, green; Co^{T}_{2c}, purple; O_{3c}, black; O_{4c}, gray; F, cyan. The empty cube indicates Co site.

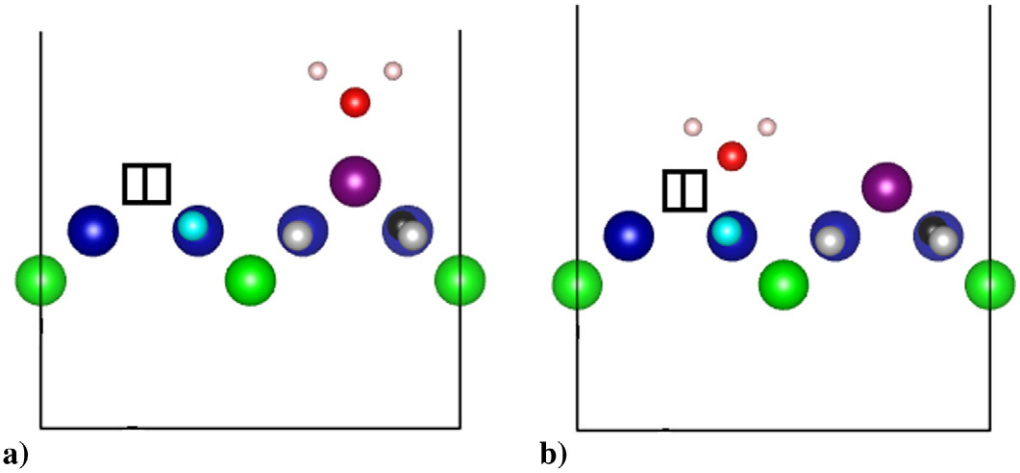

Fig. 4. Side view of H_2O adsorption at the Co^{T}_{2c} (a) and Co^{O}_{5c} (b) sites on the Co_3O_4 (100) $Co_{0.5}$-terminated surface. Color coding: Co^{O}_{5c}, blue; Co^{T}_{4c}, green; Co^{T}_{2c},purple; O_{3c}, black; O_{4c}, gray; F, cyan; O_{ads} (H_2O), red; H, white. The empty cube indicates Co site.

Zasada et al. [24] found that water molecules dissociate on twofold coordinated Co^{T}_{2c} site on the pure surface with formation of terminal hydroxyl groups (Co^{T}_{2c} — OH distance is 1.81 Å) and bridging hydroxyl groups by involving an O_{3c} surface ion with −1.18 eV adsorption energy. In our study, water adsorbs dissociatively on the Co^{T}_{2c} site on the perfect surface with energy of −1.6 eV (Co^{T}_{2c} — OH distance is 1.85 Å).

The adsorption and dissociation energy of water molecules are calculated as

$$\Delta E_{ads} = E_{adsorbate/surface} - (E_{adsorbate} + E_{surface}), \quad (14)$$

where $E_{adsorbate/surface}$, $E_{adsorbate}$ and $E_{surface}$ correspond to the total energies of a system formed by the adsorbate at the surface, the isolated adsorbate molecule in gas phase and the bare surface, respectively.

Fig. 5 presents the water dissociation geometry on the Co_3O_4 (100) $Co_{0.5}$-terminated surface.

On the fluorine-doped surface a water molecule at Co^{T}_{2c} site adsorbs without dissociation, with the small energy of −1.66 eV.

On the F-doped surface Co^{O}_{5c} site adsorption of water molecule occurs in an associative manner, the calculated adsorption energy was −1.49 eV. On a twofold coordinated Co^{T}_{2c} site on the pure surface OOH species adsorbs with the energy of 3.03 eV (Co^{T}_{2c} — O(H) distance is 1.81 Å), whereas on the Co^{O}_{5c} site OOH adsorbs with the energy of 3.26 eV and the Co^{O}_{5c} — O(H) distance of 2.08 Å. In its turn, OOH species on twofold coordinated Co^{T}_{2c} site on the fluorine-doped surface adsorbs with 2.35 eV (Co^{T}_{2c} — O(H) the distance is 1.81 Å), whereas on the Co^{O}_{5c} site OOH species adsorbs with the energy of 2.75 eV and the Co^{O}_{5c} — O(H) distance of 2.09 Å (Table 2).

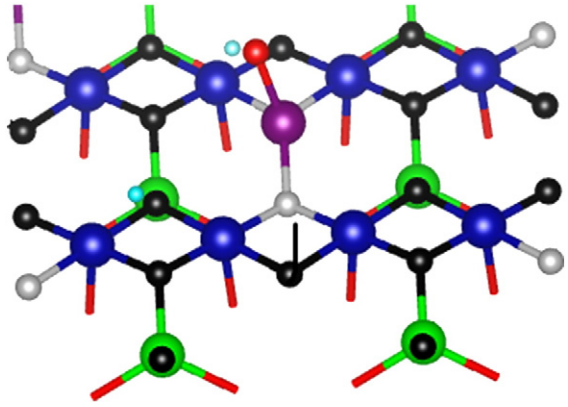

Fig. 5. Top view of dissociation geometry on the Co_3O_4 (100) $Co_{0.5}$-terminated surface. Color coding: Co^{O}_{5c}, blue; Co^{T}_{4c}, green; Co^{T}_{2c},purple; O_{3c}, black; O_{4c}, gray; O_{ads}(H_2O), red; H, cyan.

The Gibbs free energies of the reactions (1) to (4) were calculated as

$$\Delta G_i = \Delta E_i + \Delta ZPE_i - T\Delta S_i. \quad (15)$$

T is the temperature, and S_i entropy, where the binding energies of the intermediates are

$$\Delta E_{OH} = E(OH^*) - E(*) - \left[E(H_2O) - \frac{1}{2}E(H_2)\right] \quad (16)$$

$$\Delta E_O = E(O^*) - E(*) - [E(H_2O) - E(H_2)] \quad (17)$$

$$\Delta E_{OOH} = E(OOH^*) - E(*) - \left[2E(H_2O) - \frac{3}{2}E(H_2)\right]. \quad (18)$$

The binding energies of O, OH and OOH (ΔE_O, ΔE_{OH}, ΔE_{OOH}) and the bond lengths on the undoped and F-doped Co_3O_4 (100) $Co_{0.5}$-terminated surface are summarized in Table 3. We reveal that the binding energies of O*, OH* and OOH* on the cobalt oxide surface, calculated with PBE + U, scale according to the relation $\Delta E_{OOH*} = \Delta E_{OH*} + 3.2$ within ± 0.4 eV as was shown in Ref. [4,13].

We have calculated the Gibbs free energy changes along the reaction pathway using the computational standard hydrogen electrode (SHE) allowing us to replace a proton and an electron with the half a hydrogen molecule at V = 0 V vs SHE according to theory [11,13]. The theoretical overpotential is found according to the standard relation

$$\eta = \max[\Delta G_i]/e - 1.23[V]. \quad (19)$$

Fig. 6 presents the free energy changes of reactions (1) –(4) based on DFT + U calculations of adsorbed intermediates on the perfect and fluorine-doped Co_3O_4 (100) surface at 0.2 ML water coverage. The

Table 2
Basic characteristics of water adsorption process on undoped and fluorine-doped Co_3O_4 (100) $Co_{0.5}$-terminated surface. ΔE_{ads}—adsorption energy; d—dissociative mode; a—associative mode; $d_{Co-O(H2)}$—bond length in Å.* denotes present work.

Adsorption center Co^{T}_{2c}								
Undoped						F-doped		
ΔE_{ads}/eV		Adsorption type		$d_{Co-O(H_2O)}$		ΔE_{ads}/eV	Adsorption type	$d_{Co-O(H_2O)}$
*	[24]	*	[24]	*	[24]	*	*	*
−1.6	−1.18	d	d	1.85	1.81	−1.66	a	1.62

Table 3
The binding energies of O, OH and OOH (ΔE_O, ΔE_{OH}, ΔE_{OOH} in eV) and bond length on the undoped and F-doped Co_3O_4 (100) $Co_{0.5}$-terminated surface. d_x—is bond length in Å, * denotes adsorbate atom.

	ΔE_O	d_{Co-O}	ΔE_{OH}	$d_{Co-O(H)}$ $d_{O(*)-H(*)}$	ΔE_{OOH}	d_{Co-O} $d_{O(*)-H(*)}$ $d_{O(*)-O(*)}$	ΔE_O	d_{Co-O}	ΔE_{OH}	$d_{Co-O(H)}$ $d_{O(*)-H(*)}$	ΔE_{OOH}	d_{Co-O} $d_{O(*)-H(*)}$ $d_{O(*)-O(*)}$
	Adsorption center Co^T_{2c}						Adsorption center Co°_{5c}					
Undoped	2.23	1.59	−0.11	1.78 0.97	3.03	1.81 0.98 1.47	2.29	1.86	−0.09	1.79 0.97	3.26	2.08 0.98 1.45
Fluorine doped	1.81	1.6	−0.54	1.77 0.97	2.35	1.81 0.98 1.48	1.82	1.85	−0.19	1.80 0.97	2.75	2.09 0.98 1.47

calculations suggest that the theoretical overpotentials for water adsorption on the site Co^T_{2c} on the doped and F-doped surfaces are nearly the same (0.77–0.78 V). In contrast, on Co°_{5c} site at undoped surface the overpotential is 0.81 V, with the formation of O* as the determining step. However, at fluorine-doped surface the water adsorption on Co^O_{5c} site shows much smaller overpotential, only 0.44 V, with the same potential determining step as for the undoped surface. In this case the adsorption energy of O* species is strongly reduced relative to that on undoped surface, which results in decrease of the Gibbs free energy.

To elucidate in more detail the reasons for the reduced overpotential on the fluorine-doped surface and the Co^O_{5c} sites, in Table 4 are listed the Bader charges and the local magnetic moments at the Co^O_{5c} sites are presented along with the O, OH, OOH charges. The oxidation states assigned according to Ref. [9]. An initial oxidation state of the Co° changes from 3+ to 4+ for OOH species on the undoped surface, and for O on both, doped and undoped, surfaces. We neglect any additional kinetic barriers that may be present between the intermediates.

4. Conclusions

Using accurate DFT + *U* calculations, we have shown that water can be dissociatively adsorbed on the tetrahedrally coordinated Co^{2+} ions on the Co_3O_4 (100) surface. From the computed Gibbs free-energy

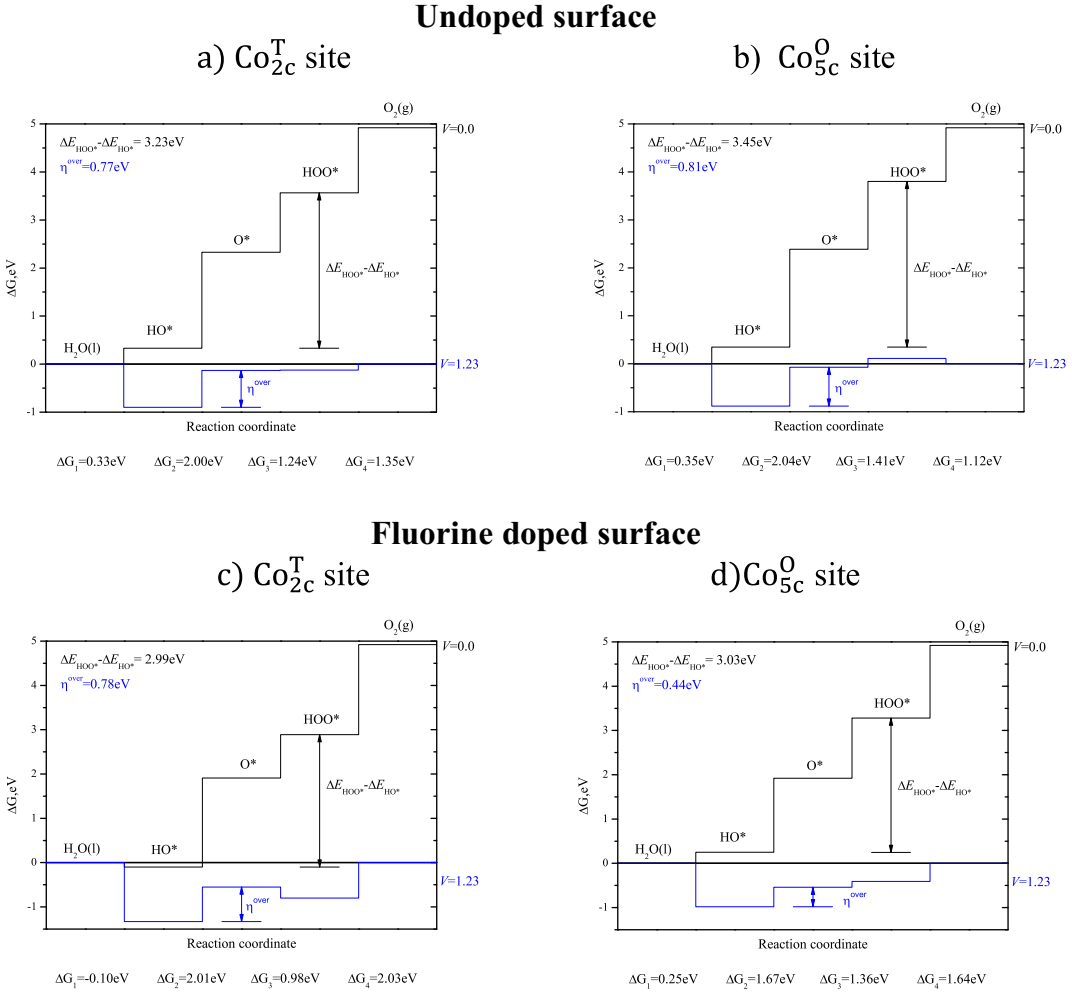

Fig. 6. Free-energy diagram at pH = 0 and T = 298 K for the four steps of the OER at $V = 0$ and $V = 1.23$ V. Results for the Co^T_{2c} and Co^O_{5c} sites at 0.2 ML water coverage for undoped and F-doped surfaces shown; For each case the characteristical difference $\Delta E_{OOH*} - \Delta E_{OH*}$ [4,13] and η^{over} are shown.

Table 4
Bader atomic charges on Co (q, *e*), and the magnetic moments (m, μ_B) on the Co^{O}_{5c} and Co^{T}_{2c} as well as charges of O, OH and OOH on the undoped and F-doped Co_3O_4 (100) $Co_{0.5}$-terminated surface. The atomic charges of regular O ions are −1.15*e*. The oxidation states of Co ions are also indicated.

$Co_{0.5}$-terminated surface		No adsorbate — (*)		OH*			O*			OOH*		
		q	|m|	q	|m|	q:OH	q	|m|	q:O	q	|m|	q:OOH
undoped	Co^{T}_{2c}	1.27 2+	2.61	1.25 2+	2.61	−0.56	1.21 2+	1.53	−0.64	1.27 2+	2.53	−0.51
	Co°_{5c}	1.46 3+	0.03	1.45 3+	0.05	−0.56	1.55 4+	1	−0.82	1.53 4+	1.32	−0.52
F-doped	Co^{T}_{2c}	0.84 2+	2.1	1.26 2+	2.6	−0.57	1.22 2+	1.53	−0.64	1.25 2+	2.55	−0.55
	Co°_{5c}	1.43 3+	0.07	1.46 3+	0.04	−0.6	1.58 4+	1.1	−0.87	1.44 3+	0.04	−0.57

changes along the OER, we found that the fluorine-doped $Co_{0.5}$-terminated Co_3O_4 (100) surface is catalytically active.

We found also that at the Co^{O}_{5c} site on fluorine-doped surface theoretical overpotential on the Co_3O_4 (100) surface is considerably reduced, from 0.81 to 0.44 V. Due to large overpotential, the OER efficiency on the pure Co_3O_4 substrate is expected to be low and thus F doping does improve it. This implies that fluorine-doped Co_3O_4 is active for electrochemical oxidation of water, in full agreement with experimental observations [10]. In the forthcoming paper we will discuss cation, Cs doping effects.

Acknowledgments

This study was partly supported by grant from Kazakhstan No. 137/2013, and Latvian ESF project Nr. 2013/0015/1DP/1.1.1.2.0/13/APIA/VIAA/010. E.K. acknowledges the Russian Science Foundation for funding the analysis of the F-doping effects under the project 14-43-00052. T.M.I. thanks the Center for Computational Materials Science, Institute for Materials Research, Tohoku University (Sendai, Japan) for their continuous support of the SR16000 M1 supercomputing system. The authors thank R. Merkle for the many stimulating discussions.

References

[1] M. Batzill, U. Diebold, Phys. Chem. Chem. Phys. 9 (2007) 2307–2318.
[2] W.-Y. Li, L.-N. Xu, J. Chen, Adv. Funct. Mater. 15 (2005) 851–855.
[3] Y. Li, B. Tan, Y. Wu, Nano Lett. 8 (2008) 265–268.
[4] M. Garcia-Mota, M. Bajdich, V. Viswanathan, A. Vojvodic, A.T. Bell, Jens K. Norskov, J. Phys. Chem. C 116 (2012) 21077–21082.
[5] P. Liao, J.A. Keith, E.A. Carter, J. Am. Chem. Soc. 134 (2012) 13296–13309.
[6] C. Ohnishi, K. Asano, S. Iwamoto, K. Chikama, M. Inoue, Catal. Today 120 (2007) 145–150.
[7] M. Garcia-Mota, A. Vojvodic, H. Metiu, I.C. Man, H.-Y. Su, M. Bajdich, J. Rossmeisl, Jens K. Norskov, ChemCatChem 3 (2011) 1607–1611.
[8] X.L. Xu, J.Q. Li, Surf. Sci. 605 (2011) 1962–1968.
[9] M. Bajdich, M. Garcia-Mota, A. Vojvodic, Jens K. Norskov, A.T. Bell, J. Am. Chem. Soc. 135 (2013) 13521–13530.
[10] A. Gasparotto, D. Barreca, D. Beermann, A. Devi, R.A. Fischer, P. Fornasiero, V. Gombac, O.I. Lebedev, C. Maccato, T. Montini, G.V. Tendello, E. Tondello, J. Am. Chem. Soc. 133 (2011) 19362–19367.
[11] J. Rossmeisl, A. Jogadottir, J.K. Norskov, J. Chem. Phys. 319 (2005) 178–184.
[12] J. Rossmeisl, Z.-W. Qu, H. Zhu, G.-J. Kroes, Jens K. Norskov, J. Electroanal. Chem. 607 (2007) 83–89.
[13] I.C. Man, H.-Y. Su, F. Calle-Vallejo, H.A. Hansen, J.I. Martínez, N.G. Inoglu, J. Kitchin, T.F. Jaramillo, Jens K. Nørskov, J. Rossmeisl, ChemCatChem 3 (2011) 1159–1165.
[14] G. Kresse, D. Joubert, Phys. Rev. B 59 (1999) 558–561.
[15] G. Kresse, J. Furthmüller, Phys. Rev. B 54 (1996) 11169–11186.
[16] P.E. Bloch, Phys. Rev. B 50 (1994) 17953–17959.
[17] J.P. Perdew, K. Burke, M. Ernzerhof, Phys. Rev. Lett. 77 (1996) 3865–3868.
[18] H.J. Monkhorst, J.D. Pack, Phys. Rev. B 13 (1976) 5188–5192.
[19] M. Methfessel, A.T. Paxton, Phys. Rev. B 40 (1989) 3616–3621.
[20] S.L. Dudarev, G.A. Botton, S.Y. Savrasov, C.J. Humphreys, A.P. Sutton, Phys. Rev. B 57 (1998) 1505–1509.
[21] F. Zasada, W. Piskorz, P. Stelmachowski, A. Kotarba, J.-F. Paul, T. Plocinski, K.J. Kurzydlowski, Z. Sojka, J. Phys. Chem. C 115 (2011) 6423–6432.
[22] J. Chen, X. Wu, A. Selloni, Phys. Rev. B 83 (2011) 245204–245207.
[23] K.J. Kim, Y.R. Park, Solid State Commun. 127 (2003) 25–28.
[24] F. Zasada, W. Piskorz, S. Cristol, J.-F. Paul, A. Kotarba, Z. Sojka, J. Phys. Chem. C 114 (2010) 22245–22253.